J. S. Afr. Inst. Min. Metall., vol. 90, no. 1.
Jan. 1990. pp. 17-26.

Simulating the production of deep-drawable AISI 430 stainless steel

by B.W. MULLER*, M.B. CORTIE*, and L.M. MATTHEWS*

SYNOPSIS

A fundamental problem that faces researchers who seek to improve industrial processes is that it is difficult to predict the consequences of changes in process routes without plant-scale trials. Clearly, a reliable means for the testing of new ideas on a small scale is desirable.

This paper describes a thermomechanical processing route for the laboratory-scale production of deep-drawable AISI 430 stainless steel. The material produced is essentially indistinguishable from commercial grades of deep-drawable AISI 430.

A modified thermomechanical processing route for enhancing the deep-drawability of the Fe-17 per cent Cr alloy is described. This alternative process route was designed from metallurgical considerations, and industrial economic factors were not considered. Nevertheless, it serves to demonstrate the influence of the process route on the deep-drawability of AISI 430, as well as the relative ease with which alternative processing routes can be simulated in the laboratory.

SAMEVATTING

'n Fundamentele probleem waarmee navorsers te kampe kry, wanneer daar gestreef word om nywerheidsprosesse te verbeter, is dat dit moeilik is om sonder aanlegskaalproewe die gevolge van veranderinge aan die prosesroete te voorspel. 'n Betroubare manier om nuwe idees op 'n klein skaal te toets is ongetwyfeld wenslik.

Hierdie referaat beskryf 'n termomeganiese verwerkingsroete vir die laboratoriumskaalproduksie van dieptrekbare vlekvrye staal AISI 430 wat in wese nie van kommersiële grade dieptrekbare AISI 430 onderskei kan word nie.

'n Gewysigde termomeganiese verwerkingsroete vir die verbetering van die dieptrekbaarheid van die Fe-17 persent Cr-legering word beskryf. Hierdie alternatiewe prosesroete is op grond van metallurgiese oorwegings ontwerp en daar is geen faktore rakende industriële ekonomie in aanmerking geneem nie. Dit demonstreer nietemin die invloed van die prosesroete op die dieptrekbaarheid van AISI 430, asook die relatiewe gemak waarmee alternatiewe verwerkingsroetes in die laboratorium nageboots kan word.

Introduction

Type 430 stainless steel is a corrosion-resisting ferritic material that contains about 17 per cent chromium and less than 0,1 per cent carbon. This alloy is considerably cheaper than austenitic stainless-steel grades such as type 304. Although the deep-drawability of type 430 is adequate for many purposes, it is not as good as that of type 304, for example. However, unlike most grades of austenitic stainless steel, type 430 is virtually immune to chloride-induced stress corrosion. Deep-drawable type 430 is used typically for cooking ware and items such as kitchen sinks. Although type 430 is less expensive than the 300-series stainless steels, this is somewhat offset by disadvantages such as a greater susceptibility to pitting corrosion, inferior press formability, poor toughness, and a limited weldability.

This paper examines the mechanical properties of type 430, particularly the properties that are known to affect deep-drawability. It was necessary to simulate the production of commercial-quality type 430 in the laboratory before a study could be made of the effect of small changes to either the alloy composition or the processing route. The work described in this paper therefore consists of three parts: a determination of the typical properties of commercial deep-drawable type 430, the replication of this material in the laboratory and, finally, the application of the thermomechanical simulation methodology to demonstrate the beneficial effects of a modified thermomechanical processing route.

* Mintek, Private Bag X3015, Randburg, 2125 Transvaal.
© The South African Institute of Mining and Metallurgy, 1990. Paper received 9th June, 1989. SA ISSN 0038-223X/3.00 + 0.00.

Experimental

Materials

The properties of commercial deep-drawable type 430 were determined from samples of material that were obtained from Middelburg Steel & Alloys, from a Japanese manufacturer, and from a West German manufacturer. These producers are denoted here as A, B, and C respectively. The material was supplied in the form of sheets 0,8 mm thick.

The experimental materials were made in a vacuum-induction furnace from raw material that was supplied by Middelburg Steel & Alloys. The chemical analyses of the four materials are given in Table I.

Thermomechanical Processing

Table II shows two of the process routes that were examined. Route A was intended to produce material similar to commercial-grade material, and was based on both published[2,3] and unpublished[4] information. Route B was designed to develop an enhanced favourable crystallographic texture in the material. The rationale behind Route B will be discussed later.

Rolling was undertaken on a laboratory rolling mill with a capacity of 150 t and a roll peripheral speed of 0,5 m/s. The plates were pickled after each annealing in 20 per cent hydrochloric acid kept at 80°C, and then

TABLE I
CHEMICAL COMPOSITION OF FIVE ALLOYS EXAMINED (IN PERCENTAGES BY MASS)

Element*	A	B	C	Route A	Route B
Cr	16,7	16,1	15,7	16,1	16,5
Ni	0,13	0,09	0,20	0,14	0,15
Si	0,6	0,5	0,3	0,5	0,6
Mn	0,6	0,3	0,5	0,5	0,6
Cu	0,11	0,04	0,06	0,08	0,09
Mo	<0,02	<0,02	0,10	<0,02	<0,02
C	0,07	0,09	0,07	0,06	0,07
N	0,05	0,01	0,04	0,03	0,04
Ferrite† factor	12,58	14,14	11,30	13,94	13,90

* For all the alloys, the sulphur content was 0,01 per cent, and the oxygen and phosphorus content 0,02 to 0,03 per cent
† After Kaltenhauser[1]

TABLE II
TWO OF THE THERMOMECHANICAL PROCESS ROUTES EXAMINED

Route A	Route B
Melt in vacuum-induction furnace	Slab cast at Middelburg Steel
	Hot-roll to 40 mm
	Anneal at 820°C for 30 min
Soak at 1150°C, 3 h	Cold-roll to 37 mm
Hot-roll from 40 to 4 mm	Anneal at 820°C for 90 min
(4 passes, finish at 700°C)	Cold-roll to 27 mm
Reheat to 720°C, roll to 2,7 mm	Anneal at 820°C, 75 min
(4 passes, finish about 680°C)	Cold-roll to 18,8 mm
	Anneal at 820°C, 30 min
Anneal at 820°C, 1,5 h	Cold-roll to 9,8 mm
Cold-roll to 0,81 mm	Anneal at 820°C, 45 min
Anneal at 820°C, 3 min	Cold-roll to 2,8 mm
	Anneal at 820°C, 30 min
Surface finish, roll to 0,79 mm	Cold-roll to 0,8 mm
Final anneal at 820°C, 80 s	Anneal at 820°C, 3 min

swabbed with 30 per cent nitric acid to give a bright finish to the plates.

Metallography

The optical microscopy involved conventional techniques of sample preparation, which were followed by etching. Table III lists three of the etchants that were used.

TABLE III
ETCHANTS FOR TYPE 430 STAINLESS STEEL

Feature required	Etchant
Microstructure	60 ml H_2O, 80 ml HCl, 5 g CuCl, 50 ml ethanol, 10 ml Teepol
Grain size	Electrolytic etch in concentrated HNO_3
Carbides	10% (by mass) ammonium persulphate in H_2O

The Heyn intercept method was used in the determination of grain size, and the result was converted to an American Society for Testing & Materials (ASTM) grain-size number[5].

Mechanical Properties

Tensile-strength tests were conducted in specimens cut from the sheets at 0, 30, 45, 60, and 90 degrees from the rolling direction. *R* values, a reliable indication of deep-drawability[6], were determined after the specimens had been subjected to a strain of 10 per cent. Other tensile-test parameters were determined with the aid of an Instron computer-controlled test system and commercially available software. A cross-head speed of 2 mm/min was used in all the tests.

Texture Analysis

The crystallographic texture of the sheets, a factor that directly controls the deep-drawability of the material[7], was determined on a Siemens X-ray diffractometer with the use of a molybdenum tube and commercially available software. A crystallographic texture is said to be present in a polycrystalline material when the crystallographic planes within individual grains are not randomly orientated with respect to some macroscopic axis. This is usually found in highly deformed material such as wire or sheet, since deformation occurs more readily along certain slip planes and directions within individual grains.

Two methods of representing the preferred orientation are used in this paper: probability values (P-values) and pole diagrams.

Probability Values. Probability values are calculated according to the method described by Pickering[8] for ferritic stainless steels. In this study, the *P* value was calculated by use of the Bragg diffracted intensities of six families of crystallographic planes: {110}, {200}, {211}, {220}, {013}, and {222}. Since the {110} and {220} planes are parallel, the values obtained for these were averaged. The *P* values vary between 1 and 5. A value of 1 indicates a completely random orientation, and a value greater than 1 indicates that a large number of grains have those particular planes parallel to the measuring plane, which, in this work, was the rolling plane. The *P* value is used as a rapid indication of texture changes, as well as in the assessment of the influence of texture on deep-drawability. A high P_{111}:P_{100} ratio is associated with a high *R* value.

Pole Diagrams. Pole diagrams are essentially maps that indicate the number of planes, from a particular family of planes (for example {100}), that lie at particular angles to some reference direction of the specimen. For wrought products, the reference directions are usually the rolling (RD), transverse (TD), and normal (ND) directions. The angles, which are easily visualized in three dimensions (Fig. 1), are plotted in two dimensions with the use of the standard stereographic projection. The number of planes in this orientation is related to the Bragg diffracted X-ray intensity obtained at those angles. A sample with no texture (such as a powder specimen) will have equal intensity over the whole figure. Wrought products, which usually have a preferred orientation, will then show higher intensities at particular angles, indicating that the particular planes are lying at those angles with respect to the RD, ND, and TD directions. A texture is described by {hkl} <uvw>, where {hkl} is the plane parallel to the rolling plane, and <uvw> is the direction parallel to the rolling direction[9].

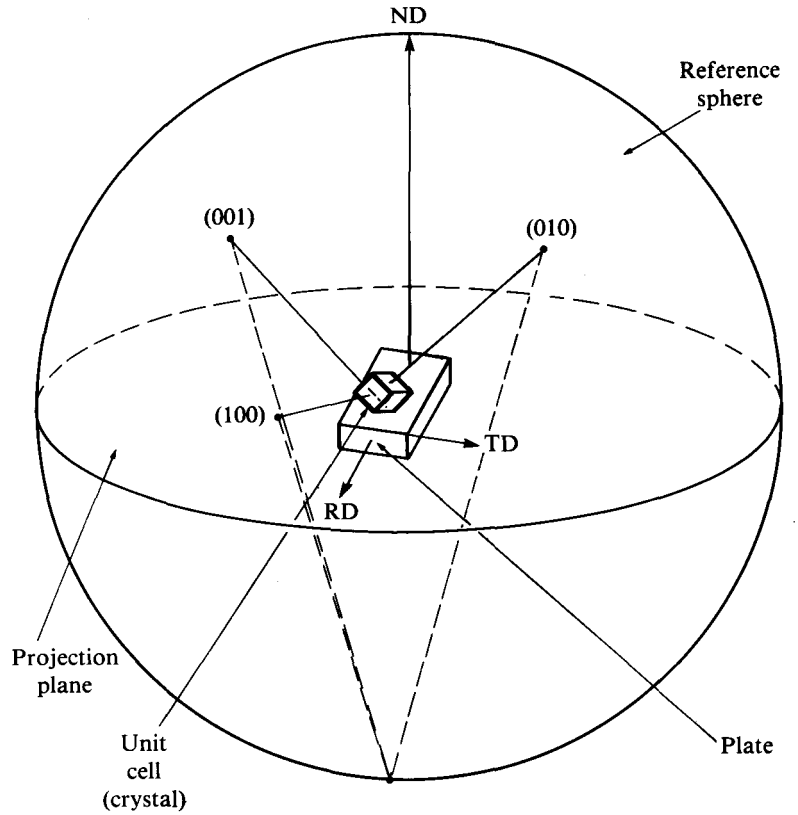

Fig. 1—Schematic representation of the construction of a pole diagram

Corrosion Testing

Corrosion tests were carried out according to the G5–78 ASTM standard. The environment consisted of 1N sulphuric acid at 25°C purged with high-purity nitrogen. The samples consisted of disks of approximately 16 mm in diameter with a surface finish of 1200 grit. The measurements of potentiodynamic anodic polarization were started after the sample had been immersed for 30 minutes. The plot started 250 mV below the corrosion potential, and proceeded through 1,30 V against the standard calomel electrode. The sweep rate was 0,1 mV/s.

Microstructure of Commercial Products

The commercial products showed a variation in grain size from 2,5 to 15 μm within each sample. The average grain size of 8 to 9 μm gave an ASTM grain-size number of between 10 and 11. For comparison, the grain size of the material produced in the laboratory was ASTM 11. Fig. 2 shows the microstructure of Producer A's material. The material of Producer B was identical to that of A, but that of Producer C possessed a bimodal distribution of grain size, with fine grains at the surface and larger grains in the interior. This indicates that, after annealing, the material received a final cold reduction followed by a short annealing. This may have contributed to the excellent surface finish found in this material.

Development of Microstructure in Simulated Type 430

The evolution of the microstructure of the experimentally produced material was studied from the stage of the cast ingot to the final 0,8 mm thick sheets.

The as-cast material consisted principally of ferrite and martensite, which indicates that this particular melt had passed through the two-phase austenite-plus-ferrite field during cooling. Carbides were observed, particularly on the ferrite–martensite grain boundaries, and these were identified by potentiostatic etching as $M_{23}C_6$.

An example of the microstructure of the material after it had been hot-rolled is shown in Fig. 3. Large, flattened grains (ASTM grain-size 8 in the normal direction) are present, and there is a pronounced banded structure. During annealing, recrystallization and grain growth occurred, and this is shown in Fig. 4. The carbides remain distributed in stringers, but these are no longer associated exclusively with grain boundaries.

Cold-rolling induced gross deformation of the grains and, in addition, dispersed the carbides to a greater extent. The first annealing of the cold-rolled plate resulted in recrystallization and grain growth of the cold-worked structure. Fig. 5 shows the equiaxed, fine-grained microstructure of the final product. The carbides still have some sign of directionality, although the banding has been reduced considerably.

Corrosion Resistance

The results of the corrosion tests are set out in Table IV. The potentiodynamic plots did not reveal a great variation between the samples of the various producers and the experimental-grade material. This was expected, since the chemical composition is similar for all four materials that were investigated. The corrosion potential is identical for the four materials, while most of the corrosion parameters that were calculated for the experimentally produced deep-drawable type 430 fall within the scatter band of the commercial-grade materials.

Crystallographic Texture of the Commercial Products

The crystallographic texture of the three commercial

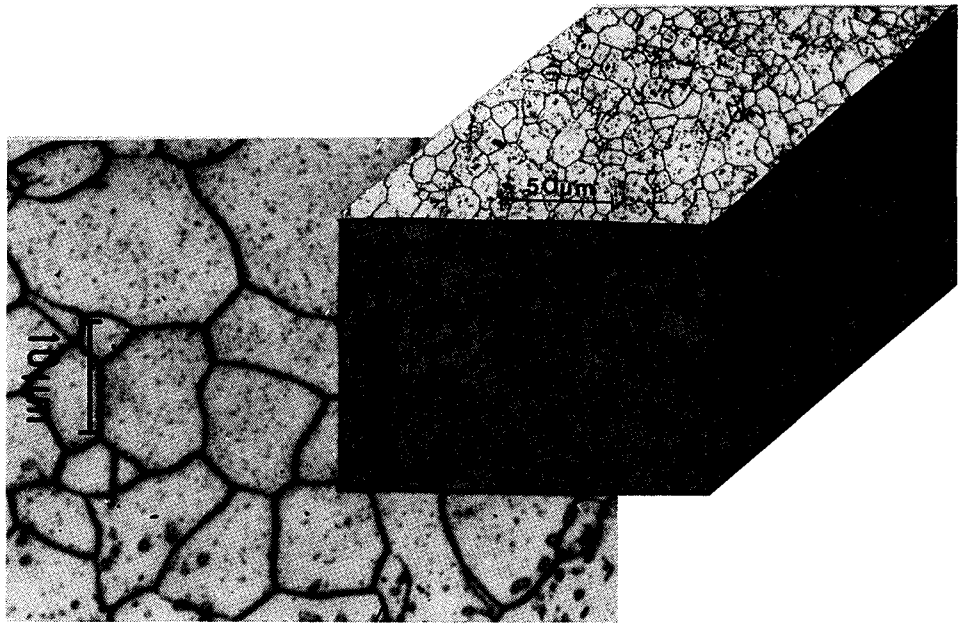

Fig. 2—Typical microstructure of commercial deep-drawable type 430 (Producer A)

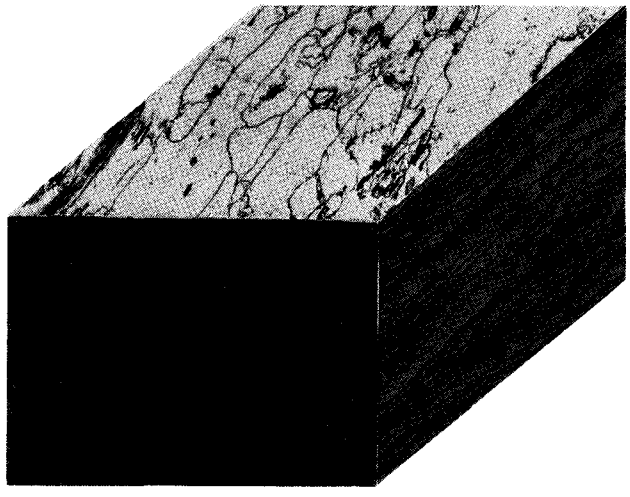

Fig. 3—Large, flattened grains caused by hot-rolling

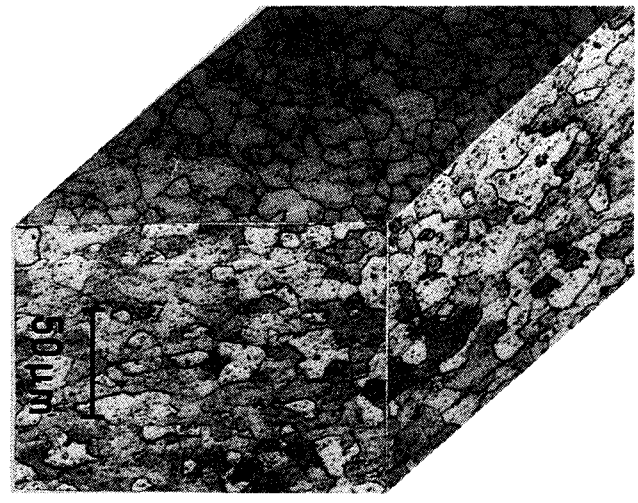

Fig. 5—The equi-axed structure of the 0,8 mm sheet produced in the laboratory

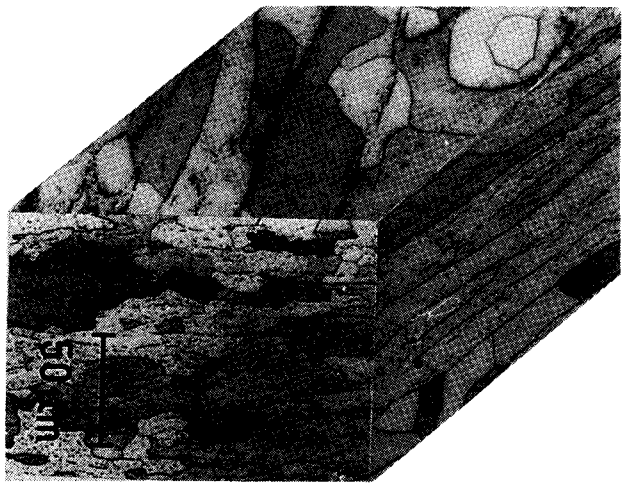

Fig. 4—The effect of recrystallization and grain growth on a hot-rolled structure

TABLE IV
RESULS OF CORROSION TESTS
Environment: 1N sulphuric acid solution Test conditions: ASTM G5-78

Item	MSA	Japan	Germany	Experiment
CORR POTE (mV)	−500	−500	−500	−500
CORR I (Micro A per $cm^2$4)	1350	1000	900	2060
PASS I (Micro A)	3,35	3,16	1,12	1,64
CRIT I (Micro A)	6000	11200	5000	8000

products that were studied is shown in the pole figures of Figs. 6, 7, and 8. As can be seen, the material of Producer A and Producer B contained similar textures. In both cases, the materials consisted mainly of $\{111\}<1\bar{1}0>$ and $\{111\}<11\bar{2}>$ textures. Although the highest contour levels correspond to $\{111\}<1\bar{1}0>$ and the $\{111\}<11\bar{2}>$ orientations, the high-intensity contours are spread out between the ideal orientations. This is typical of the $\{111\}<uvw>$ fibre textures found in the body-centred-cubic metals that are used for deep-drawing applications. The $\{110\}$/RD fibre is indicated but is very weak, and is probably a remnant of the hot-rolling textures.

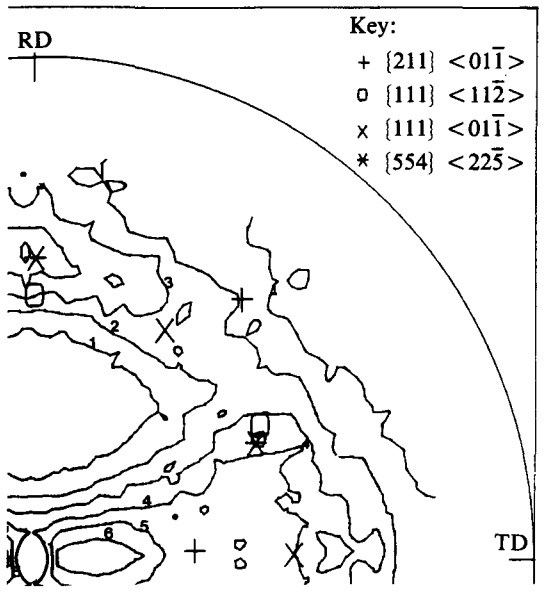

Fig. 6—{100} pole diagram for the material of Producer A

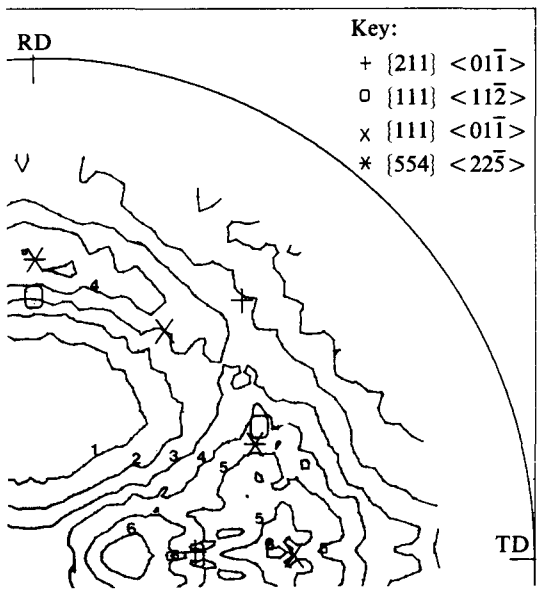

Fig. 7—{100} pole diagram for the material of Producer B

The material of Producer C differed from the other two. Its most prominent texture was $\{554\}<22\bar{5}>$, which is close to $\{111\}<11\bar{2}>$. Less-pronounced textures that could be seen were the $\{001\}<110>$ and $\{211\}<1\bar{3}1>$

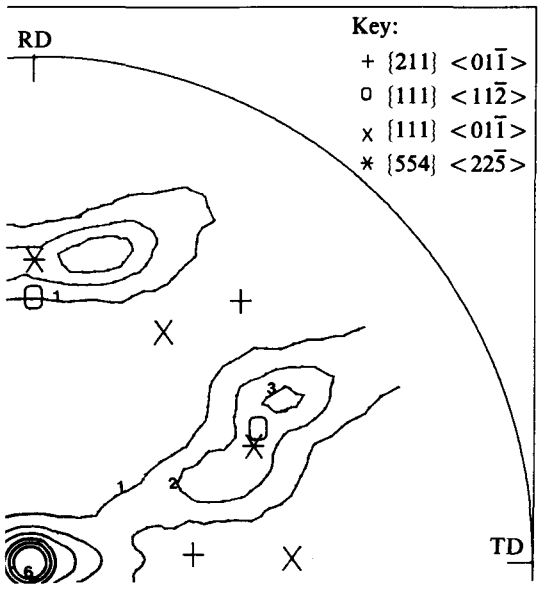

Fig. 8—{100} pole diagram for the material of Producer C

textures. There is clearly no $\{111\}<uvw>$ fibre texture in the material of Producer C.

Development of Texture in Experimental Type 430

The effect of the various process steps on the development of texture in the type 430 material that was produced in the laboratory is depicted in Fig. 9, which shows the changes in the *P* values of the five planes that were considered. It can be seen that cold-rolling made the most important contribution to the development of the desirable $\{111\}$ texture. This texture is similar to the texture obtained in aluminium-killed steels[10], and is associated with the formation of recrystallization nuclei at carbides or inclusions.

The texture of the material produced in the laboratory, which was intended to simulate industrial grades of deep-drawable type 430, is shown in Fig. 10. The material has a $\{111\}<uvw>$ fibre texture, which has the $\{554\}<225>$ as its strongest component. The texture is similar to that of the samples of Producers A and B, except for a slightly stronger enhancement of the $\{554\}<225>$ component (which is close to $\{111\}<112>$) within the fibre. Again, there are indications (high contours in the centre region of the pole figure) that the $\{110\}$/RD fibre is present. In this case, the presence of the fibre is known to originate from hot-rolling.

Enhanced Texture in Route B Material

Since cold-rolling was the most important factor in the development of the advantageous $\{111\}$ texture, the thermomechanical processing route given in Table II and denoted as Route B was attempted. The $\{100\}$ pole figure, which was measured after this processing route, is shown in Fig. 11. A very well-developed $\{111\}<uvw>$ texture was immediately identified (high contour levels forming an almost complete circle). Particular components such as $\{111\}<112>$ are not prominent, which demonstrates that there is a complete rotation of grains within the rolling plane. The $\{011\}$/RD fibre is also strongly reduced by the excessive cold-rolling.

The pronounced $\{111\}<uvw>$ fibre texture of the

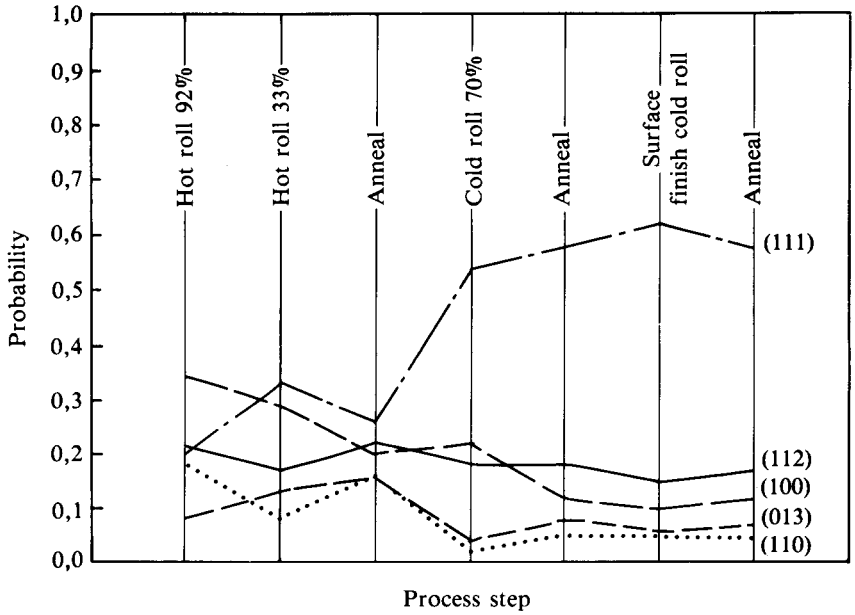

Fig. 9—Development of preferred orientation during the laboratory production of type 430

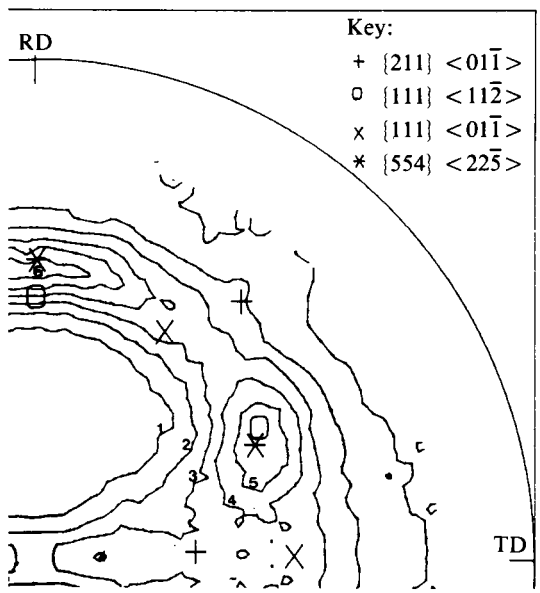

Fig. 10—{100} pole diagram for type 430 manufactured in the laboratory

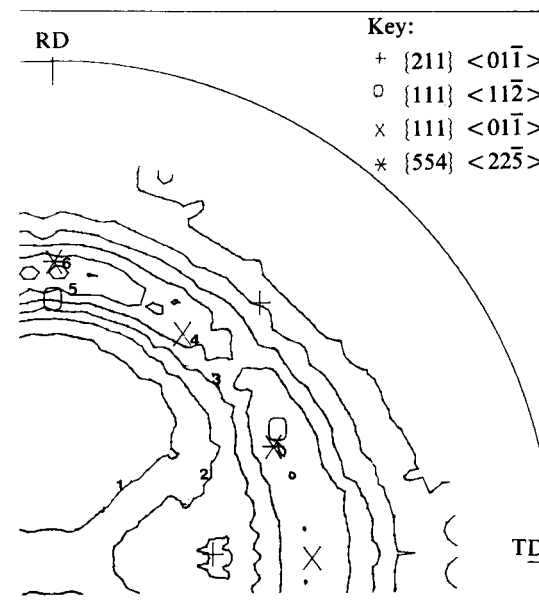

Fig. 11—{100} pole diagram for Route B material

Route B material is noticeable, especially when the *P* values of the five planes are plotted in the form of a bar chart. Fig. 12 compares the condition of the three commercial materials with that of the simulated (Route A) type 430, as well as with the specially processed Route B material.

Mechanical Properties

Tensile Strength

Fig. 13 compares the proof stress, and Fig. 14 the ultimate tensile stress, of the three commercial materials with that of the simulated (Route A) type 430. Since all these materials have a preferred crystallographic orientation, the mechanical properties vary with the direction of testing. In the graphs that follow, the mechanical properties were plotted against the angle from the rolling direction. It can be seen that the laboratory material had essentially the same proof and tensile stress as those of the commercial grades.

Measures of Deep-Drawability

Two good indications of the deep-drawability of a material are the *R* value and the strain-hardening coefficient. Figs. 15 and 16 illustrate the variations of these properties for the three commercial grades that were examined, as well as for the simulated (Route A) type 430. It is clear that the laboratory material falls within the scatter band of the commercial-grade materials. In addition, Erichson cupping tests carried out on the simulated type 430 showed it to have similar properties to the type 430 of Middelburg Steel & Alloys.

The Route B material was found to have a high *R*

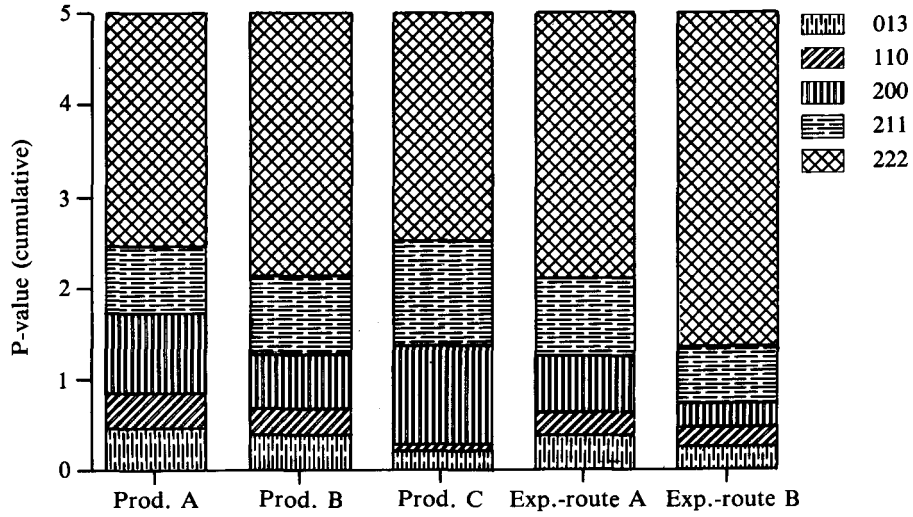

Fig. 12—Probabilities that a given plane lies parallel to the surface of the rolled sheet

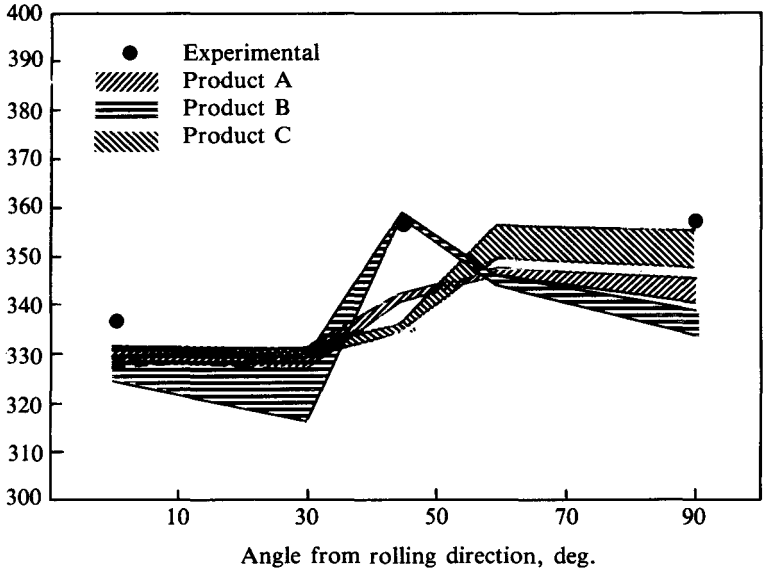

Fig. 13—Variation of proof stress with rolling direction

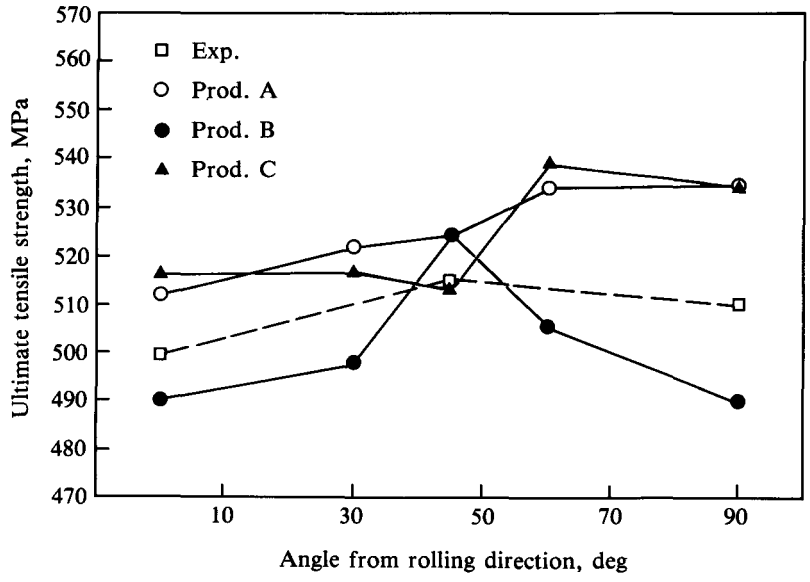

Fig. 14—Variation of ultimate tensile stress with rolling direction

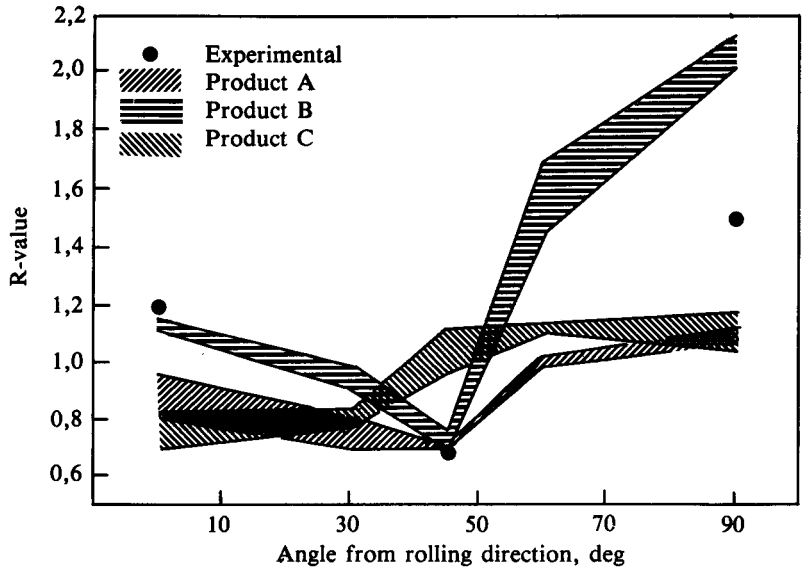

Fig. 15—Variation of the plastic strain ratio with rolling direction

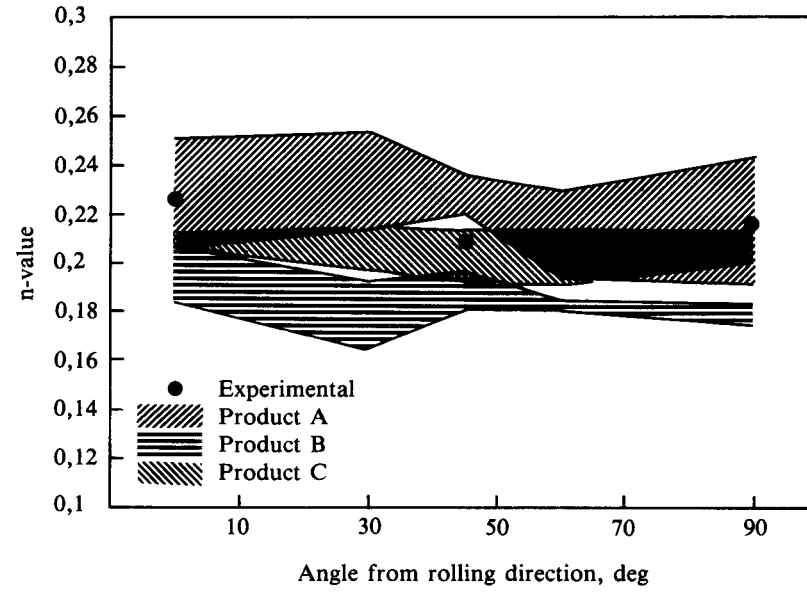

Fig. 16—Variation of the strain-hardening coefficient with rolling direction

value, which indicates that it should possess excellent deep-drawability. The *R* values of the five materials studied at 0° to the rolling direction is given in Table V, as well as several other material properties considered to influence formability.

TABLE V
MECHANICAL PROPERTIES AT 0° TO THE ROLLING DIRECTION

Property	Product A	Product B	Product C	Route A	Route B
R	0,87	1,15	0,77	1,18	1,59
n	0,23	0,20	0,21	0,23	0,22
Proof	330	329	330	337	352
Ultimate tensile strength	512	490	516	500	532
Elongation, %	30	32	27	42	35

Discussion

Development of Texture

A comparison of the pole figures of the two experimental alloys indicates a difference in the texture development associated with the two routes. Successive cold-rolling and annealing enhance the {111}<uvw> type fibre texture, which is associated with high *R* values. Since it was observed that the {111} textures are enhanced after annealing, it is believed that annealing in combination with rolling makes the most important contribution to this enhancement. However, it is also clear that significant cold reductions are required to introduce the {111}<uvw> type texture.

The Estimation of Deep-Drawability from Texture Data

It is known that on-line measurements of texture are being made by some producers of steel sheets[11]. From such information it should be possible to control the

quality and, in particular, the formability of the product. Crystallographic texture can, in principle, be measured more accurately than the R, n, and Erichson values, which are often used in industry, since a single determination of crystallographic texture is the product of thousands of individual measurements. In addition, the determination of texture can be carried out non-destructively and in 'real time'.

The qualitative correlation between crystallographic texture—especially the {111} texture—and good formability in ferritic steels has already been discussed. However, there is an incentive to relate the crystallographic texture in a quantitative fashion to the deep-drawability of a material. Although various schemes, some fairly complex, have been described in the literature[6,7], three simple empirical methods were examined at Mintek.

The qualitative correlation between a high P_{111} value and a high R value in a material has already been discussed. Accordingly, a simple model in which the R value depends in a linear fashion on the P_{111} value was first attempted. This produced an expression of the form

$$R \text{ value} = a + b.P_{111}. \quad \text{.....} \quad (1)$$

Pickering, on the other hand, has proposed that the R value can be best correlated with the logarithm of the ratio of the P_{111} value to the P_{100} value[8]. This produces an expression of the following form:

$$R \text{ value} = a + b.\log(P_{111}/P_{100}). \quad \text{.....} \quad (2)$$

A third proposal, made by Muller[12], states that the R value can be correlated with the difference between the sum of the vector components of the five planes parallel to the sheet surface, and the sum of the components perpendicular to the surface. This suggests that

$$R \text{ value} = 1/a.\Sigma_1^n\ [P_{hkl} * (\cos(T) - \sin(T))], \quad \text{.....} \quad (3)$$

where T is taken as the smallest angle between plane {kkl} and the {111} plane.

Each of these three methods was applied to the data on texture, and R values were obtained for the seven materials that were produced during the course of the present work. The results are shown in Table VI. The first, and simplest, method yielded the best statistical fit for the present data.

TABLE VI

COMPARISON OF THREE SCHEMES FOR THE ESTIMATION OF DEEP-DRAWABILITY FROM DATA ON CRYSTALLOGRAPHIC TEXTURE

Scheme	a	b	Correlation coefficient (r)	% Variance explained
P_{111}	−0,281	0,424	0,83	69
$\ln(P_{111}/P_{100})$	0,645	0,309	0,79	62
P_{hkl}	3,513	–	0,82	67

The empirical model, which uses the P_{111} value, is plotted in Fig. 17. The outer broken lines are the 95 per cent confidence intervals for the mean predicted R value, and were obtained with the use of standard statistical techniques[13]. The fit of the model is encouraging, but more data must be added before the approach can be verified.

Conclusions

A comparison of the microstructure, crystallographic texture, and mechanical properties of the laboratory-produced material showed its properties to be effectively similar to those of the overseas grades.

The crystallographic texture of the West German material is noticeably different from that of the South African and Japanese materials.

The development of both the microstructure and the crystallographic texture during the simulated production of type 430 stainless steel showed that the greatest increase in texture favourable to deep-drawing occurs during cold-rolling.

The mechanical properties of type 430 stainless steels vary with the angle of the specimen to the rolling direction. This variation was determined for several proper-

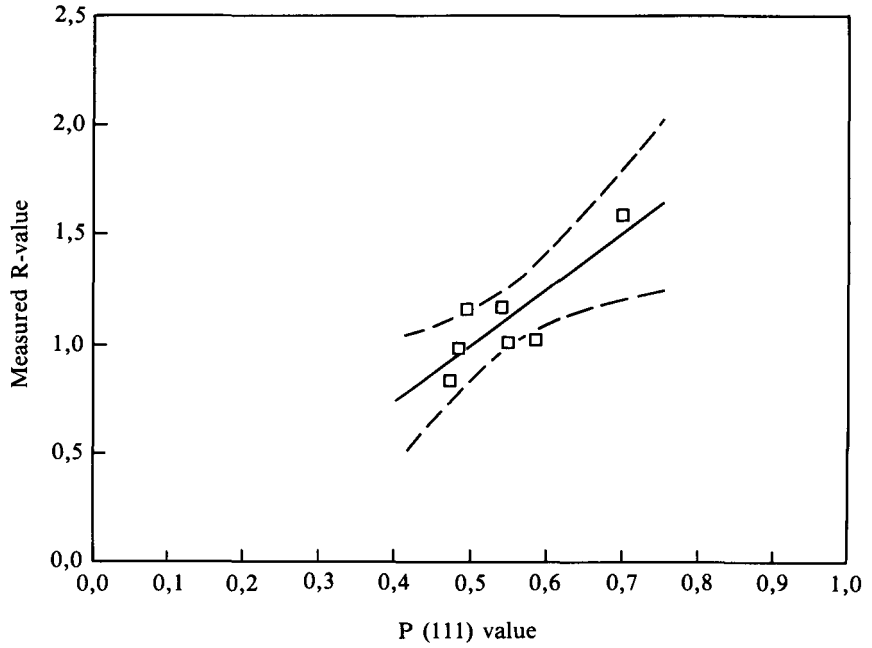

Fig. 17—Empirical model using the P_{111} value

ties, including the proof strength, the tensile strength, and the R value.

The most favourable texture from the point of view of deep-drawability occurs when the {111} planes of individual grains are parallel to the surface. The simplest measure of this condition is the P_{111} value.

An exploration of three of the empirical relationships that correlate deep-drawability with crystallographic texture indicated that it is possible to estimate the R value of a type 430 stainless steel from its P_{111} value.

The modified thermomechanical processing route used, which consists of alternating cold-rolling and annealing, demonstrated the beneficial effect of cold-rolling. The {111} texture and deep-drawability of the resultant material are considerably greater than those normally found in industrially produced grades.

Acknowledgements

This paper is published by permission of Mintek and Middelburg Steel & Alloys (Pty) Ltd.

References

1. KALTENHAUSER, R.H. Improving the engineering properties of ferritic stainless steels. *Metall. Engng Q.*, vol. 11, no. 2. May 1971. pp. 41–47.
2. SAWANTANI, T., ISHII, M., YOSHIMURA, H., ASHIURA, T., YAMAMOTO, A., and WAKAMUTSA, M. Development of continuous annealing process for 17%Cr stainless steel. *New developments in stainless steel technology*, Sep. 1984. pp. 269–282.
3. MCGANNON, H.E. (ed.). *The making, shaping and treating of steel.* United States Steel, 9th Edition. 1971. pp. 1163–1191.
4. Private communication. Middelburg, Middelburg Steel & Alloys, 1987, 1988.
5. VAN DER VOORT, G.F. *Metallography, principles and practice.* New York, McGraw-Hill, 1984.
6. DIETER, G.E. *Mechanical metallurgy.* Second edition. New York, McGraw-Hill, 1981.
7. HELD, J.F. *Mechanical working and steel processing 4.* Paper 3. New York, The Metallurgical Society of AIME, 1965.
8. PICKERING, F.B. Physical metallurgical development of stainless steels. *Perspectives in metallurgical development.* London, ION, 1984. pp. 1–27.
9. BUNGE, H.J. *Texture analysis in materials science. Mathematical methods.* London, Butterworth, 1982.
10. HUTCHINSON, W.B. Development and control of annealing texture in low-carbon steels. *International Metals Review*, vol. 29, no. 1. 1984. pp. 25–42.
11. BOTTCHER, W., and KOPINECK, H.J. Uber ein Rontgentexturmessverfahren zur Zerstorungsfreien 'on-line'-Bestimmung technologischer Kennwerte von Kaltgewalzten Stahlbandern. *Stahl und Eisen*, vol. 105, no. 9. 1985. pp. 509–516.
12. MULLER, B.W. The processing route required to produce deep drawable type 430 stainless steel. Technikon Witwatersrand, thesis for the Master's Diploma in Technology, Sep. 1988.
13. SPIEGEL, M.R. *Schaum's outline of theory and problems of statistics.* New York, McGraw-Hill, 1972.

CRS publications

These publications are available from the Centre for Resource Studies, Queen's University, Kingston, Ontario K7L 3N6, Canada.

● *Federal and provincial taxation of the Canadian mining industry: Impact and implications for reform,* by R.W. Boadway, K.J. McKenzie, and J.M. Mintz. 190 pp. $35.00.

The tax treatment of the mining industry and the design of appropriate tax policies is of considerable importance for Canada, in view of the special role this industry plays in the economy. This study examines how the existing system of income taxation and provincial mining taxation impinges on incentives to invest in mining at all stages from initial exploration to final depletion and sale. The authors' other task is to determine what type of tax reforms would both satisfy government-revenue requirements and remove the adverse effects of the existing system on the industry.

● *Metals demand and the Canadian metal industry: Structural changes and policy implications,* by C. Nappi. 135 pp. $20.00.

Demand for and prices of metals have turned around in recent years from slack demand and low prices to tight supplies and record high prices. This study investigates reasons for changes in demand, examining in detail both cyclical and structural causes, and identifies enduring trends. The author discusses the implications for the strategies of metals firms and for government policies, warning industry decision-makers against assuming that markets will remain strong without conscious and deliberate efforts at marketing and product development.

● *Marketing of nonferrous metals,* edited by L.M. Jackson and P.R. Richardson. 131 pp. $25.00.

This volume contains the papers presented at the 19th CRS Policy Discussion Seminar, which addressed a range of topics related to marketing.

Among the many challenges facing metal producers are the development of substitutes such as plastics and ceramics, health and environmental concerns, shifting markets, expanding production from third-world competitors, and worldwide political and economic instability. Most of the industry has failed to adapt to changing world markets. Responsibility for this failure to re-orient business strategy was attributed to top management's 'sales' mentality, which directs their efforts towards taking market share from other producers and closes their minds to the notion of expanding the market. Product and market development were generally regarded as the most effective method of protecting nonferrous metals against the encroachment of substitutes and extending their life cycles.